Axle-Less F_1-ATPase Rotates in the Correct Direction

Shou Furuike,[1]* Mohammad Delawar Hossain,[1,2]* Yasushi Maki,[3] Kengo Adachi,[1] Toshiharu Suzuki,[4,5] Ayako Kohori,[1] Hiroyasu Itoh,[6,7] Masasuke Yoshida,[4,5] Kazuhiko Kinosita Jr.[1]†

F_1–adenosine triphosphatase (ATPase) is an ATP-driven rotary molecular motor in which the central γ subunit rotates inside a cylinder made of three α and three β subunits alternately arranged. The rotor shaft, an antiparallel α-helical coiled coil of the amino and carboxyl termini of the γ subunit, deeply penetrates the central cavity of the stator cylinder. We truncated the shaft step by step until the remaining rotor head would be outside the cavity and simply sat on the concave entrance of the stator orifice. All truncation mutants rotated in the correct direction, implying torque generation, although the average rotary speeds were low and short mutants exhibited moments of irregular motion. Neither a fixed pivot nor a rigid axle was needed for rotation of F_1-ATPase.

F_1-ATPase, a water-soluble portion of the enzyme ATP synthase, has been predicted (*1*, *2*) and proved (*3*) to be an ATP-driven rotary motor. Its minimal subcomplex, active in ATP hydrolysis and rotation, consists of $\alpha_3\beta_3\gamma$ subunits (*4*, *5*), which we refer to here as F_1. A crystal structure (*6*) of bovine mitochondrial F_1 (MF_1) is shown in Fig. 1A. The central γ subunit is supported by the $\alpha_3\beta_3$ cylinder at the top orifice and bottom (blue and dark green atoms); the bottom support forms a hydrophobic sleeve that could act as a bearing (*7*). Three catalytic sites for ATP hydrolysis reside at α-β interfaces, primarily hosted by a β subunit. In the original structure (*7*), one site (hosted by β_{TP} and α_{TP} in Fig. 1) bound an ATP analog; another (β_{DP} and α_{DP}), adenosine 5′-diphosphate (ADP); the third (β_E and α_E), none; and noncatalytic nucleotide-binding sites in the other interfaces bound the ATP analog. The upper portions of β_{TP} and β_{DP} are bent toward, and apparently push, the top of the γ shaft, whereas β_E retracts and pulls the shaft (Fig. 1A). This structure led Wang and Oster (*8*) to propose a push-pull rotary mechanism in which the γ shaft, which is slightly bent and skewed, makes a conical rotation around the axis shown in black in Fig. 1A. In this mechanism, pivoting of the shaft in the bottom support is essential for torque production. Here, we ask if the pivot, or even the whole shaft, is necessary for rotation.

We used as the wild type a modified (α-C193S, β-His_{10} at N terminus, γ-S107C, γ-I210C) subcomplex (*9*) of thermophilic F_1 (TF_1). Following earlier work (*10*) on *Escherichia coli* F_1 (EF_1), we previously deleted 21 C-terminal residues of TF_1-γ. The mutant (γ-ΔC21 in Fig. 1B) produced considerable torque (*11*), but the truncated rotor tip would still touch the bottom support (Fig. 1A), and thus the remaining bottom interactions might have provided the torque. Beyond 21 residues, we failed to obtain an active subcomplex. Here, we find that shorter γ subunits, the shortest two being almost outside the stator cavity (Fig. 1), are expressed at levels similar to that of the wild type (fig. S1), and that we can obtain assembled subcomplexes containing a mutated γ subunit, albeit at lower yields for short mutants (Fig. 2), by omitting heat treatment in the purification procedure and doing column treatments at room temperature (*12*).

We tested if these mutants rotate, by attaching the β subunits to a glass surface through the histidine residues at the N terminus and putting, as a marker, a 40-nm gold bead or its duplex on the two cysteines of the γ subunit. All mutants, up to γ-ΔN22C43 (Fig. 1, E and F), could rotate the bead in the correct, counterclockwise (viewed from above in Fig. 1) direction for >100 revolutions (Fig. 3A). The probability of finding a rotating bead was low for short mutants: from the wild type up to γ-ΔN7C29, we observed, on average, a few or more rotating beads per field of view (7.1 μm by 7.1 μm) when 5 to 10 nM F_1 was infused into the observation chamber at 2 mM ATP; about 0.5 bead per field of view for 10 to 20 nM γ-ΔN11C32; >10 beads per chamber (~6 mm by 18 mm) for 40 nM γ-ΔN14C36; and 1 or 2 beads per chamber for 40 to 100 nM γ-ΔN18C40 or 100 nM γ-ΔN22C43. For the last two mutants, surface bead density was very low, suggesting that most F_1 molecules lacked γ, consistent with the faint γ bands in Fig. 2. The beads that rotated relatively smoothly without much surface obstruction gave time-averaged rotary speeds that were consistent with the rate of ATP hydrolysis (Fig. 4B). The hydrolysis rate leveled off at the value of γ-less mutant $\alpha_3\beta_3$, which shows hydrolysis activity uncoupled to γ rotation (*13*). The paucity of γ in samples of the shortest mutants (Fig. 2) explains this asymptotic behavior.

The time-averaged rate of rotation, as well as the rate of ATP hydrolysis, was low in the truncated mutants (Fig. 4B), indicating that the interactions between the γ tip and the lower stator support are important for rapid progress of catalysis. We note the relatively flat portion in Fig. 4B between γ-ΔC21 and γ-ΔN7C29, where the tip would be unable to make strong contacts with the lower support; from γ-ΔN11C32, for which the tip would be completely in the middle of the cavity, the rates decreased again, and we observed irregular movements as described below. We have shown previously that reverse rotation of F_1 by an external force leads to reversal of chemical reactions in the catalytic sites, leading to net ATP synthesis (*14*). The reversal by manipulation of the γ angle alone implies a γ-dictator mechanism, whereby the γ angle controls which chemical reaction takes place in the three catalytic sites: ATP binding, hydrolysis, and product release (*5*, *15*). Leverage by a short γ, without firm pivoting at the bottom, will be inefficient in driving β (and α) subunits over an activation barrier into the conformation appropriate for the next chemical reaction. A remote possibility is that the $\alpha_3\beta_3$ cylinder alone may undergo ATP-dependent, circular conformational changes without supervision by γ, and that a bead, or even the shortest γ, simply reflects this motion. With $\alpha_3\beta_3$, however, we did not find any bead to rotate. The correlation between the γ length and rotary speed (Fig. 4B) indicates the diminishing but finite contribution of a short γ in the coordination.

At a sufficiently high camera speed, all rotations appeared stepwise even at 2 mM ATP (Fig. 3, C and D). For the wild-type protein, dwells at this saturating ATP concentration are at ~80° past an ATP-waiting angle, where ATP hydrolysis and phosphate release take ~1 ms each at room temperature (*9*, *15*, *16*). The dwelling angles of the mutants have not been assigned. The steps of mutants were noisy, indicating larger fluctuation of short γ subunits, and some mutants showed two or more dwelling angles per 120°. The horizontal lines in Fig. 3, C and D, show the angles of the most populated dwells in each mutant. The dwells imply the presence of an activation barrier(s) against a reaction that is to take place at that angle.

In addition to the apparently thermal fluctuations, short mutants exhibited irregular motions where the bead moved toward and stayed near the rotation axis for tens of milliseconds before going back to the rotary track mostly onto the position 120° ahead (Fig. 3B-b), occasionally onto the previous position (Fig. 3B-c), and rarely but notably onto the position 120° backward (Fig. 3B-d). Such behaviors tended to be repetitive, but the total time was usually short and

[1]Department of Physics, Faculty of Science and Engineering, Waseda University, Shinjuku-ku, Tokyo 169-8555, Japan. [2]Department of Physics, School of Physical Sciences, Shahjalal University of Science and Technology, Sylhet-3114, Bangladesh. [3]Department of Physics, Osaka Medical College, Osaka 569-8686, Japan. [4]Chemical Resources Laboratory, Tokyo Institute of Technology, Nagatsuta 4259, Yokohama 226-8503, Japan. [5]ATP-Synthesis Regulation Project, International Cooperative Research Project (ICORP), Japan Science and Technology Agency (JST), Aomi 2-41, Tokyo 135-0064, Japan. [6]Tsukuba Research Laboratory, Hamamatsu Photonics KK, Tokodai, Tsukuba 300-2635, Japan. [7]Core Research for Evolutional Science and Technology (CREST) "Formation of Soft Nano-Machines" Team 13*, Tokodai, Tsukuba 300-2635, Japan.

*These authors contributed equally to this work.
†To whom correspondence should be addressed. E-mail: kazuhiko@waseda.jp

within the width of the vertical bars in Fig. 3A. Exceptionally long repetitions were also observed (Fig. 3A, two long horizontal rectangles). The bead position near the rotation axis suggests an F_1 conformation(s) quite different from the one in Fig. 1. If the two cysteines on γ (near the black circles in Fig. 1F) bound the bead, a central bead location would require the γ head to become upright, by counterclockwise inclination in Fig. 1F, right. The tip of the γ shaft would then move toward α_{DP}, a movement allowed for a short γ. Alternatively, the coiled-coil portion of a short γ may occasionally melt. To be upright, the γ head must reposition itself in the concave orifice, breaking all γ-stator interactions seen in the crystal. The F_1 would be in an unclutched state. This scenario based on the wild-type MF_1 structure may not be valid, but some major reorganization must underlie the central bead location.

The shortest mutant (γ-ΔN22C43) exhibited frequent irregular motions and also backward steps (Fig. 3A). It still rotated mainly in the correct direction, which must be driven by an effective positive torque. For the upper and lower curves in Fig. 3A, there were 65 and 44 moments of irregular motion in 100 s, respectively, with the total durations of 2.7 and 2.4 s; there were 368 and 259 forward 120°-steps, compared with 32 and 37 backward steps. The second shortest γ (γ-ΔN18C40), which is also nearly outside the stator cavity, rotated much more steadily.

To estimate the torque of the mutants, we attached larger beads for which the viscous friction is high. γ-ΔC21 could rotate a duplex of 0.49-μm polystyrene beads with an apparent torque of ~20 pN·nm (*11*), about half the torque of the wild type, but the mutant was unable to rotate a 0.9-μm bead duplex. γ-ΔN4C25 up to γ-ΔN11C32 could rotate a 0.29-μm duplex, but not the 0.49-μm duplex. Rotating duplexes were rare for γ-ΔN7C29 and γ-ΔN11C32, and they tended to detach from the surface during observation. The 0.29-μm bead, compared with the 40-nm gold bead, likely bumps the glass (or F_1) surface and is detached. When the bead is stuck against a surface in one of the dwelling angles where the activation barrier is high for short mutants, the bead may stop there.

Assuming that the instantaneous rotary speeds of the 0.29-μm bead duplexes during 120° steps are determined by the balance between the torque of the motor and viscous friction (*3*, *5*, *17*), we estimated the torque of γ-ΔN4C25 to γ-ΔN11C32 to be ~20 pN·nm (fig. S3A). This estimate may be questioned because the mutants undergo extensive thermal fluctuations and thus 120° excursions may result from occasional large-amplitude fluctuations that are not directly related to the motor torque (a diffusion-and-catch mechanism of rotation). In some duplexes, we observed three 120° steps occurring always in succession (Fig. 4A, arrow), presumably because the F_1 was obliquely attached to the surface. Torque estimated in the 360° excursions (fig. S3B), which cannot be entirely thermal, was at least 8 pN·nm. Also, most duplexes in Fig. 4A rotated with a time-averaged speed exceeding 1 revolution s^{-1},

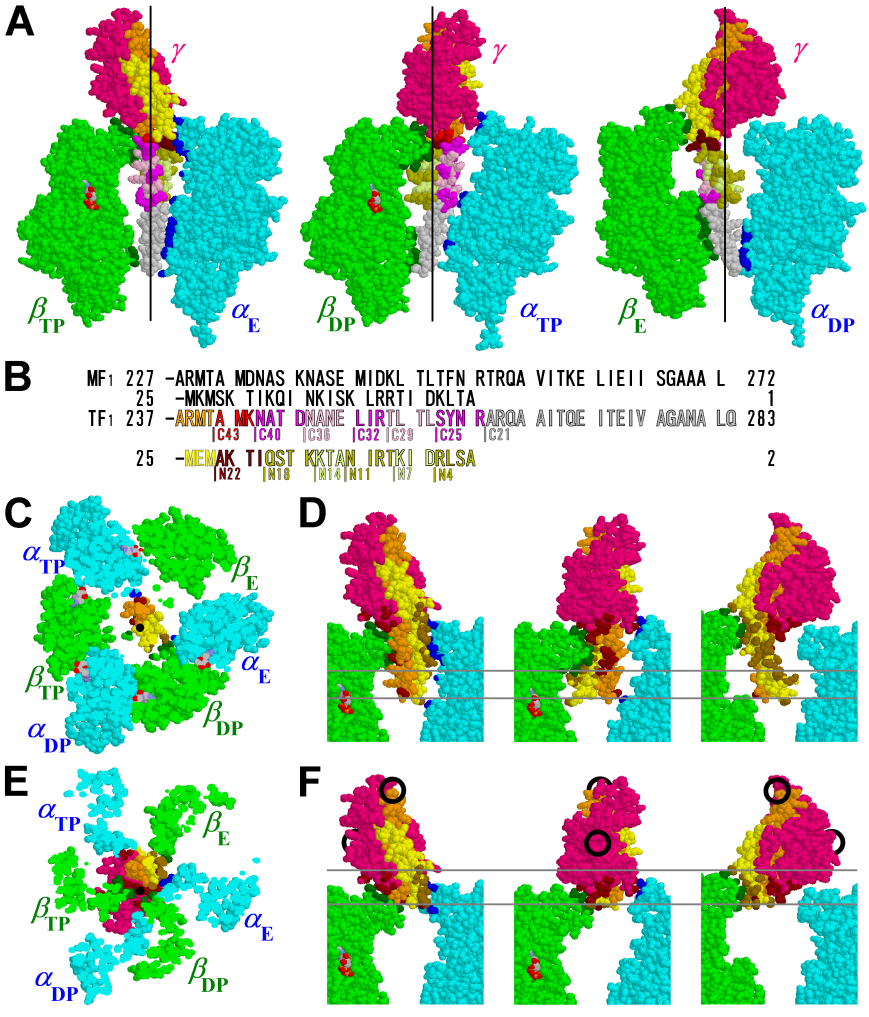

Fig. 1. An atomic structure (*6*) of MF_1. (**A**) Side views showing the central γ subunit and an opposing α-β pair. The membrane-embedded F_o portion of ATP synthase would be above the γ subunit. Truncations of the γ subunit are shown with the color scheme in (B); the N- and C-terminal α helices are in yellow and orange, respectively. Those atoms of α and β subunits that are within 0.5 nm from an atom of γ (excluding hydrogens) are colored blue and dark green, respectively. Nucleotides are shown in CPK colors. Black lines [and black dots in (C) and (E)] represent a putative rotation axis (*8*). (**B**) Amino acid sequences at the C and N termini of γ in MF_1 (*22*) and TF_1, except that the numbering in (B) starts from Met-1, which is absent in the expressed wild-type protein (*23*). Abbreviations for the amino acid residues are as follows: A, Ala; D, Asp; E, Glu; F, Phe; G, Gly; I, Ile; K, Lys; L, Leu; M, Met; N, Asn; Q, Gln; R, Arg; S, Ser; T, Thr; V, Val; and Y, Tyr. (**C** to **F**) Structures of γ-ΔN4C25 (C and D) and γ-ΔN22C43 (E and F). For γ-ΔN4C25, γ-Met-4 is represented by γ-Lys-4, excluding the ε-amino group to mimic Met. For γ-ΔN22C43, γ-Met-22 is represented by γ-Ser-22. (C) and (E) are bottom views of the section between the gray lines in (D) and (F). Atoms of γ that are within 0.5 nm from an atom of α or β are shown in gold and brown (there were none on the C-terminal helix of γ-ΔN22C43). Black circles in (F) show approximate locations of biotinylated cysteines.

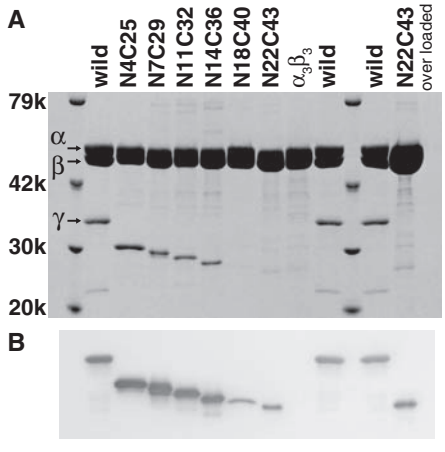

Fig. 2. Confirmation of γ truncations by polyacrylamide gel electrophoresis. (**A**) A 12.5% gel containing 0.1% SDS, stained with Coomassie Brilliant Blue R-250. (**B**) Western blot of (A) stained with antibodies to the γ subunit.

implying a lower bound for the effective torque of 2 pN·nm. Torque of the shorter mutants could not be estimated, but the unidirectional character of the rotation implies production of an effective torque in the correct direction.

Most manmade rotary machines rely on a rigid axle held by a static bearing: thanks to the constraint exerted by the bearing, almost any force acting on the axle is converted to a torque through a lever action. Nature seems to have adopted this simple principle for the bacterial flagellar motor (*18*) and the proton-driven F_o motor of the ATP synthase (*4*): Their rotor axis is held stationary by stator bearings, and thus force from one driving unit, acting on only one point on the rotor, suffices to produce torque. For the short γ mutants here, however, the concept of a rigid axle in a static bearing no longer applies. Yet the mutants do rotate.

Rotating the shortest γ is perhaps like rotating an unsupported pen between six fingers, suspending the pen vertically at the very top. The six upper tips of the α and β subunits must play three roles in a highly concerted fashion: moving the rotor in the correct direction, serving as a fulcrum to convert the motion into torque, and preventing the truncated rotor from escaping. All these functions require contacts between the rotor and tips, but static contacts do not allow full rotation. The grip must be dynamic, yet continuous; a failure for a moment will allow Brownian motion to carry the rotor away. A partial hint may be the ~30° twist of γ in some crystal structures (*19*); the rest of a 120° step might be covered by Brownian rotation. The short γ may indeed be driven by biased diffusion,

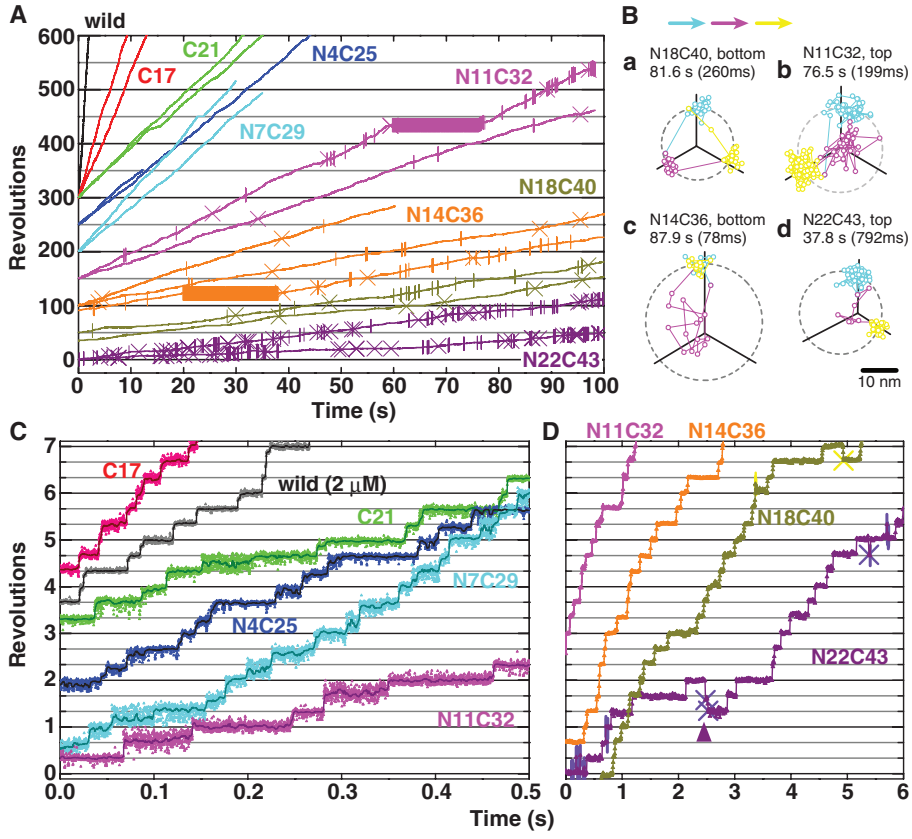

Fig. 3. Rotation of 40-nm gold beads attached to the γ subunit. Counterclockwise rotations, viewed from above in Fig. 1A, are plotted as positive revolutions. ATP concentration was 2 mM except for the wild-type protein in (**C**). (**A**) Overall time courses for beads that rotated relatively fast. Vertical bars and two horizontal rectangles indicate the period during which irregular motions described in (B) continued. Crosses indicate occurrence of a ~120° backward step, whether rotational or via irregular motion (B-d). (**B**) Traces of typical irregular motions where the bead tended to dwell near the rotation center. (a) Regular 120° steps; (b) center then forward; (c) center and turning back; (d) center then backward. (**C**) Stepping kinetics observed at 8000 frames s^{-1}. Thin dark lines, after 15-point median filtering. Most-populated angles for each mutant (judged over the entire time courses) are on the horizontal lines separated by 120°; for the wild type at 2 μM ATP, these are ATP-waiting angles. (**D**) Stepping kinetics of the shortest four mutants at 125 frames s^{-1} (records taken at higher speeds have been averaged in 8-ms bins). Vertical bars show moments of irregular motions. Crosses, backward steps; arrowhead, succession of two backward steps (a rare event).

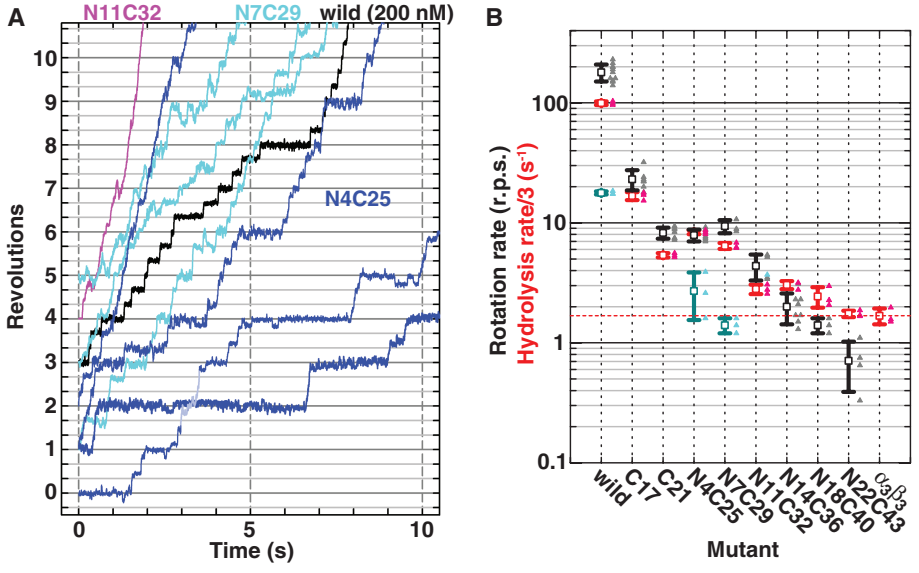

Fig. 4. (**A**) Rotation time courses for 0.29-μm bead duplexes at 500 frames s^{-1}. Data show relatively fast rotation or clearer stepping. ATP concentration was 2 mM (200 nM for the wild type). (**B**) Summary of rotation and hydrolysis rates at 2 mM ATP. Black symbols show mean ± SD for time-averaged rotation rates of 40-nm gold beads that rotated relatively fast; rates of individual beads over >50 (mostly >100) consecutive revolutions are shown in gray triangles. Dark cyan, mean ± SD for rotation rates of 0.29-μm bead duplexes that rotated relatively fast; cyan, individual rates over 10 revolutions. Red, mean ± SD for the rate of ATP hydrolysis (fig. S2); three determinations in magenta; red dashed line, mean hydrolysis rate of $\alpha_3\beta_3$. Temperature, 23°C.

as in the single-head linear motor KIF1A (*20*) that cannot rely on alternating firm grips allowed for two-head motors. Unlike KIF1A, which diffuses widely, however, diffusion of the truncated γ is largely within 120°, and most 120° steps are in the forward direction (~90% in γ-ΔN22C43 and >99% in γ-ΔN18C40). The orifice somehow blocks backward diffusion, ensuring generation of an effective torque. Clarifying how this is achieved will provide a new paradigm for the design of molecular machines. Why is there superfluous robustness in the rotary mechanism of F_1? Perhaps this began as a clumsy device, and then proceeded to sophistication. If so, ring-shaped AAA+ ATPases may all, in principle, be capable of producing torque, as suggested for helicases (*21*).

References and Notes

1. P. D. Boyer, W. Kohlbrenner, in *Energy Coupling in Photosynthesis*, B. R. Selman, S. Selman-Reimer, Eds. (Elsevier, Amsterdam, 1981), pp. 231–240.
2. F. Oosawa, S. Hayashi, *Adv. Biophys.* **22**, 151 (1986).
3. H. Noji, R. Yasuda, M. Yoshida, K. Kinosita Jr., *Nature* **386**, 299 (1997).
4. M. Yoshida, E. Muneyuki, T. Hisabori, *Nat. Rev. Mol. Cell Biol.* **2**, 669 (2001).
5. K. Kinosita Jr., K. Adachi, H. Itoh, *Annu. Rev. Biophys. Biomol. Struct.* **33**, 245 (2004).
6. C. Gibbons, M. G. Montgomery, A. G. W. Leslie, J. E. Walker, *Nat. Struct. Biol.* **7**, 1055 (2000).
7. J. P. Abrahams, A. G. W. Leslie, R. Lutter, J. E. Walker, *Nature* **370**, 621 (1994).
8. H. Wang, G. Oster, *Nature* **396**, 279 (1998).
9. R. Yasuda, H. Noji, M. Yoshida, K. Kinosita Jr., H. Itoh, *Nature* **410**, 898 (2001).
10. M. Müller, O. Pänke, W. Junge, S. Engelbrecht, *J. Biol. Chem.* **277**, 23308 (2002).
11. M. D. Hossain *et al.*, *Biophys. J.* **90**, 4195 (2006).
12. See supporting material on *Science* Online.
13. K. Miwa, M. Yoshida, *Proc. Natl. Acad. Sci. U.S.A.* **86**, 6484 (1989).
14. H. Itoh *et al.*, *Nature* **427**, 465 (2004).
15. K. Adachi *et al.*, *Cell* **130**, 309 (2007).
16. K. Shimabukuro *et al.*, *Proc. Natl. Acad. Sci. U.S.A.* **100**, 14731 (2003).
17. N. Sakaki *et al.*, *Biophys. J.* **88**, 2047 (2005).
18. H. C. Berg, *Annu. Rev. Biochem.* **72**, 19 (2003).
19. V. Kabaleeswaran, N. Puri, J. E. Walker, A. G. W. Leslie, D. M. Mueller, *EMBO J.* **25**, 5433 (2006).
20. Y. Okada, H. Higuchi, N. Hirokawa, *Nature* **424**, 574 (2003).
21. S. S. Patel, K. M. Picha, *Annu. Rev. Biochem.* **69**, 651 (2000).
22. J. E. Walker *et al.*, *J. Mol. Biol.* **184**, 677 (1985).
23. S. Ohta *et al.*, *Biochim. Biophys. Acta* **933**, 141 (1988).

24. We thank M. Shio for designing a stable microscope stage; K. Shiroguchi and A. Shinohara for gene engineering; R. Shimo-Kon and R. Kanda for sample preparation; N. Sakaki, Y. Onoue, and T. Okamoto for technical support; K. Sakamaki and M. Fukatsu for encouragement and lab management; and members of the Kinosita lab for help and advice. This work was supported by Grants-in-Aid for Specially Promoted Research and for Young Scientists (B) and the 21st Century Center of Excellence Program from the Ministry of Education, Sports, Culture, Science and Technology, Japan.

Supporting Online Material

www.sciencemag.org/cgi/content/full/319/5865/955/DC1
Materials and Methods
Table S1
Figs. S1 to S3
References
Movies S1 to S6

4 October 2007; accepted 19 December 2007
10.1126/science.1151343

A Mouse Model of Mitochondrial Disease Reveals Germline Selection Against Severe mtDNA Mutations

Weiwei Fan,[1,2] Katrina G. Waymire,[1,2] Navneet Narula,[3] Peng Li,[4] Christophe Rocher,[1,2] Pinar E. Coskun,[1,2] Mani A. Vannan,[4] Jagat Narula,[4] Grant R. MacGregor,[1,5,6] Douglas C. Wallace[1,2,7]*

The majority of mitochondrial DNA (mtDNA) mutations that cause human disease are mild to moderately deleterious, yet many random mtDNA mutations would be expected to be severe. To determine the fate of the more severe mtDNA mutations, we introduced mtDNAs containing two mutations that affect oxidative phosphorylation into the female mouse germ line. The severe *ND6* mutation was selectively eliminated during oogenesis within four generations, whereas the milder *COI* mutation was retained throughout multiple generations even though the offspring consistently developed mitochondrial myopathy and cardiomyopathy. Thus, severe mtDNA mutations appear to be selectively eliminated from the female germ line, thereby minimizing their impact on population fitness.

The maternally inherited mitochondrial DNA (mtDNA) has a high mutation rate, and mtDNA base substitution mutations have been implicated in a variety of inherited degenerative diseases including myopathy, cardiomyopathy, and neurological and endocrine disorders (*1*, *2*). Paradoxically, the frequency of mtDNA diseases is high, estimated at 1 in 5000 (*3*, *4*), yet only a few mtDNA mutations account for the majority of familial cases (*2*). Because mutations would be expected to occur randomly in the mtDNA, the paucity of the most severe mtDNA base substitutions in maternal pedigrees suggests that the severe mutations may be selectively eliminated in the female germ line.

To investigate this possibility, we have developed a mouse model in which the germline transmission of mtDNA point mutations of different severity could be tested. An antimycin A–resistant mouse LA9 cell line was cloned whose mtDNA harbored two homoplasmic (pure mutant) protein-coding gene base change mutations: one severe and the other mild. The severe mutation was a C insertion at nucleotide 13,885 (13885insC), which created a frameshift mutation in the NADH dehydrogenase subunit 6 gene (*ND6*). This frameshift mutation altered codon 63 and resulted in termination at codon 79 (Fig. 1A, top; fig. S1A, bottom). When homoplasmic, this mutation inactivates oxidative phosphorylation complex I (*5*). The mild mutation was a missense mutation at nucleotide 6589 (T6589C) in the cytochrome c oxidase subunit I gene (*COI*) that converted the highly conserved valine at codon 421 to alanine (V421A) (fig. S1A, top). When homoplasmic, this mutation reduces the activity of oxidative phosphorylation complex IV by 50% (*6*, *7*).

LA9 cells homoplasmic for both the *ND6* frameshift and *COI* missense mutations were enucleated, and the mtDNAs were transferred by cytoplast fusion to the mtDNA-deficient (ρ^o) mouse cell line LMEB4, generating the LMJL8 transmitochondrial cybrid (*8*). LMJL8 mitochondria exhibited no detectable oxygen consumption when provided with NADH-linked complex I substrates (fig. S1B) and no detectable complex I enzyme activity (fig. S1C). However, the same mitochondria exhibited a 43% increase in succinate-linked respiration and a 91% increase in complex II + III activity as well as a 62% increase in complex IV activity (fig. S1, B and C), presumably as a compensatory response to the severe complex I defect (*9*). Relative to LM(TK^-) cells, mouse L cell lines homoplasmic for the *COI* missense mutation also showed increased reactive oxygen species (ROS). Cells homoplasmic for both the *ND6* frameshift and *COI* missense mutations produced fewer ROS than did the *COI* mutant cells. However, cells that were 50% heteroplasmic for both the *ND6* frameshift and the *COI* missense mutations had the highest ROS production (fig. S1D).

To analyze the fates of the severe *ND6* frameshift versus moderate *COI* missense mtDNA mutations, we introduced these mutations into the mouse germ line. LMJL8 cybrids were enucleated and the cytoplasts fused to the mouse female embryonic stem (ES) cell line

[1]Center for Molecular and Mitochondrial Medicine and Genetics, University of California, Irvine, CA 92697, USA. [2]Department of Biological Chemistry, University of California, Irvine, CA 92697, USA. [3]Department of Pathology, University of California, Irvine, CA 92697, USA. [4]Division of Cardiology, Department of Medicine, University of California, Irvine, CA 92697, USA. [5]Department of Developmental and Cell Biology, University of California, Irvine, CA 92697, USA. [6]Developmental Biology Center, University of California, Irvine, CA 92697, USA. [7]Departments of Ecology and Evolutionary Biology and Pediatrics, University of California, Irvine, CA 92697, USA.

*To whom correspondence should be addressed. E-mail: dwallace@uci.edu